Science and Technology of Advanced Materials

ISSN: (Print) (Online) Journal homepage: www.tandfonline.com/journals/tsta20

Ion-pairing assemblies of π-extended anion-responsive organoplatinum complexes

Yohei Haketa, Yu Murakami & Hiromitsu Maeda

To cite this article: Yohei Haketa, Yu Murakami & Hiromitsu Maeda (06 Feb 2024): Ion-pairing assemblies of π-extended anion-responsive organoplatinum complexes, Science and Technology of Advanced Materials, DOI: 10.1080/14686996.2024.2313958

To link to this article: https://doi.org/10.1080/14686996.2024.2313958

Publisher: Taylor & Francis & The Author(s). Published by National Institute for Materials Science in partnership with Taylor & Francis Group.

Journal: *Science and Technology of Advanced Materials*

DOI: 10.1080/14686996.2024.2313958

Ion-pairing assemblies of π-extended anion-responsive organoplatinum complexes

Yohei Haketa, Yu Murakami, Hiromitsu Maeda*

Department of Applied Chemistry, College of Life Sciences, Ritsumeikan University, Kusatsu 525–8577, Japan

Hiromitsu Maeda maedahir@ph.ritsumei.ac.jp Department of Applied Chemistry, College of Life Sciences, Ritsumeikan University, Kusatsu 525–8577, Japan

Ion-pairing assemblies of π-extended anion-responsive organoplatinum complexes

Pt^{II} complexes of π-extended dipyrrolyldiketones were synthesized as anion-responsive π-electronic molecules. The dipyrrolyldiketone Pt^{II} complexes exhibited red-shifted absorption and photoluminescence properties. In the solid state, [1+1]-type anion complexes formed charge-by-charge ion-pairing assemblies when combined with countercations. Detailed theoretical studies of the packing structures revealed favorable interactions between the planar anion complexes and π-electronic cations.

Keywords: Pt^{II} complexes, anion-responsive π-electronic systems, ion-pairing assemblies

Subject classification codes:

1. Introduction

π-Electronic systems exhibit fascinating electronic and electrooptical properties based on the tunable electronic states that affect their absorption and luminescence properties. The assembly of π-electronic systems in an ordered arrangement results in a variety of supramolecular nanoarchitectonics [1,2] to show unique electrooptical properties that cannot be observed in single molecules [3–7]. In particular, the solid-state photophysical properties of π-electronic systems depend on the stacking arrangement of their components. Among the various solid-state luminescent materials, organoplatinum(II) complexes exhibit various photoluminescence properties such as intense phosphorescence from triplet excited states [8–13]. Assemblies with an ordered arrangement of organoplatinum(II) complexes are suitable for the applications in light-emitting devices. Recent studies on the micro- and nanocrystals of organoplatinum(II) complexes have also exhibited triplet energy transfer and phosphorescence anisotropy

amplification [14,15]. π-Extended ligands in organoplatinum(II) complexes modulate the photophysical properties of single molecules as well as those in assembled states. Stacking of organoplatinum(II) complexes in the assembled state often interferes with photoluminescence [16]. Strategies for maintaining photoluminescence by isolating π-electronic molecules in the solid state have been reported [17,18]. The introduction of bulky substituents to the peripheral ligands prevents the Pt^{II} complexes from stacking. Furthermore, ion-pairing assemblies [19] of charged emissive species and appropriate counterions can yield photoluminescent materials (Figure 1a) [20,21]. For example, solid-state ion-pairing assemblies of non-emissive receptor–anion complexes and emissive countercations exhibit enhanced emission [22,23]. Controlling the ordered arrangement of emissive π-electronic molecules in the solid state is important for the fabrication of photoluminescent materials.

Among the various phosphorescent organoplatinum(II) complexes (e.g., **2a**, Figure 1b), dipyrrolyldiketone Pt^{II} complexes bearing arylpyridine ligands exhibit efficient anion-binding behavior via hydrogen bonding at the pyrrole NH and bridging CH (Figure 1b) [24]. Modification of arylpyridine ligands results in red-shifted phosphorescence properties [25]. The square planar dipyrrolyldiketone Pt^{II} complexes exhibit non-emissive solid states owing to the efficient π–π stacking. In contrast, ion-pairing assemblies of the anion complexes and counter alkylammonium cations show enhanced phosphorescence behavior owing to their charge-by-charge assembly mode (Figure 1a). The emissive anion complexes are spatially isolated by counter alkylammonium cations, resulting in enhanced phosphorescence derived from the monomeric anion complexes. The solid-state phosphorescence properties, such as emission wavelength, can be tuned by the π-extension of ligands. Thus far, modifications at the pyrrole α-positions of dipyrrolyldiketone Pt^{II} complexes have been

limited to the substitution with 2,6-dimethylphenyl moieties. In this study, Pt^{II} complexes of π-extended dipyrrolyldiketones were synthesized to evaluate ion-pairing assemblies of Pt^{II} complexes in their anion-binding forms with π-electronic cations.

2. Experimental section

2.1. Synthesis and characterization

2.1.1. General procedures

Starting materials were purchased from FUJIFILM Wako Pure Chemical Corp., Nacalai Tesque Inc., Tokyo Chemical Industry Co., Ltd., Sigma-Aldrich Co., and Tanaka Kikinzoku Kogyo K.K. and were used without further purification unless otherwise stated. Nuclear magnetic resonance (NMR) spectra used in the characterization of products were recorded on a JEOL ECA-600 600 MHz spectrometer. All NMR spectra were referenced to solvent. UV-visible absorption spectra were recorded on a Hitachi U-3500 spectrometer. Matrix-assisted laser desorption ionization time-of-flight mass spectrometry (MALDI-TOF-MS) was recorded on a Shimadzu Axima-CFRplus. TLC analyses were carried out on aluminum sheets coated with silica gel 60 (Merck 5554). Column chromatography was performed on Wakogel C-300.

2.1.2. 1,3-Bis(3,4-diethyl-5-phenylethynylpyrrol-2-yl)-1,3-propanedione, ***1b′****.*

In a round-bottomed flask, according to the procedure that has been modified from the previous one [26], BF_2 complex of 1,3-bis(3,4-diethyl-5-phenylethynylpyrrol-2-yl)-1,3-propanedione [27,28] **1b** (240 mg, 0.427 mmol) and $LiOH{\cdot}H_2O$ (1.31 g, 31.2 mmol) were dissolved in 1,4-dioxane (90 mL) and water (90 mL) under N_2 atmosphere. To the solution was added acetic acid (AcOH) (66 μL, 1.17 mmol). The reaction mixture was stirred at 90 °C for 2.5 h. The solution was acidified dropwise with 1 M HCl aq at pH

7. After the removal of the solvent under vacuum, the residue was then partitioned between water and CH_2Cl_2. The organic phase was dried over anhydrous Na_2SO_4, and was evaporated under vacuum. The residue was then purified by chromatography over silica gel column (Wakogel C-300; eluent: $CHCl_3$) and was recrystallized from CH_2Cl_2/*n*-hexane to give **1b´** (182 mg, 0.354 mmol, 83%) as a yellow solid. R_f = 0.75 (CH_2Cl_2). ^{1}H NMR (600 MHz, DMSO-d_6, 20 °C; diketone **1b´** was obtained as a mixture of keto and enol tautomers in the ratio of 0.59:1): δ(ppm) keto from 12.06 (br, 2H, NH), 7.53 (d, J = 7.2 Hz, 4H, Ar-H), 7.43 (t, J = 6.9 Hz, 6H, Ar-H), 4.33 (s, 2H, bridging CH_2), 2.69 (q, J = 7.8 Hz, 4H, CH_2), 2.57–2.54 (m, 4H, CH_2), 1.18–1.13 (m, 12H, CH_3); enol from 11.74 (br, 2H, NH), 7.53 (d, J = 7.2 Hz, 4H, Ar-H), 7.43 (t, J = 6.9 Hz, 6H, Ar-H), 6.49 (s, 1H, bridging CH), 2.77 (q, J = 7.8 Hz, 4H, CH_2), 2.57–2.54 (m, 4H, CH_2), 1.18–1.13 (m, 12H, CH_3). ^{13}C{^{1}H} NMR (151 MHz, DMSO-d_6, 20 °C): δ (ppm) 184.56, 176.04, 132.22, 132.09, 131.47, 131.06, 131.10, 130.84, 128.98, 128.96, 128.92, 128.52, 125.29, 122.26, 122.10, 115.05, 114.75, 94.43, 93.68, 92.29, 81.60, 81.40, 50.85, 18.08, 18.02, 17.49,17.30, 15.92, 15.75, 15.73, 15.38. MALDI-TOF-MS (% intensity): *m*/*z*: 513.3 (100), 514.3 (80), 515.3 (20). Calcd for $C_{35}H_{33}N_2O_2$ ($[M - H]^-$): 513.25.

2.1.3. 1,3-Bis(3,4-diethyl-5-(4-fluorophenyl)ethynylpyrrol-2-yl)-1,3-propanedione, ***1c´****.*

In round-bottomed flask, according to the procedure that has been modified from the previous one [26], BF_2 complex of 1,3-bis(3,4-diethyl-5-(4-fluorophenyl)ethynylpyrrol-2-yl)-1,3-propanedione [27,28] **1c** (7.4 mg, 0.012 mmol) and $LiOH \cdot H_2O$ (20.1 mg, 0.479 mmol) were dissolved in 1,4-dioxane (30 mL) and water (3 mL) under N_2 atmosphere. To the solution was added acetic acid (3.0 μL, 0.053 mmol). The reaction mixture was stirred at 90 °C for 12 h. The solution was acidified dropwise with 1 M HCl aq at pH 7. After the removal of the solvent under vacuum, the residue was then

partitioned between water and CH_2Cl_2. The organic phase was dried over anhydrous Na_2SO_4, and was evaporated under vacuum. The residue was then purified by chromatography over silica gel column (Wakogel C-300; eluent: $CHCl_3$) and was recrystallized from CH_2Cl_2/*n*-hexane to give **1c´** (5.94 mg, 0.011 mmol, 87%) as a yellow solid. R_f = 0.80 (CH_2Cl_2). ^{1}H NMR (600 MHz, DMSO-d_6, 20 °C; diketone **1c´** was obtained as a mixture of keto and enol tautomers in the ratio of 0.51:1): δ (ppm) keto from 12.05 (br, 2H, NH), 7.58–7.56 (m, 4H, Ar-H), 7.29 (t, J = 8.4 Hz, 4H, Ar-H), 4.31 (s, 2H, bridging CH_2), 2.68 (q, J = 7.8 Hz, 4H, CH_2), 2.55–2.51 (m, 4H, CH_2), 1.16–1.11 (m, 12H, CH_3); enol from 11.74 (br, 2H, NH), 7.58–7.56 (m, 4H, Ar-H), 7.29 (t, J = 8.4 Hz, 4H, Ar-H), 6.46 (s, 1H, bridging CH), 2.76 (q, J = 7.8 Hz, 4H, CH_2), 2.55–2.51 (m, 4H, CH_2), 1.16–1.11 (m, 12H, CH_3). ^{13}C{^{1}H} NMR (151 MHz, DMSO-d_6 20 °C): δ (ppm) 184.43, 175.96, 162.85, 162.81, 161.21, 161.16, 133.38, 133.32, 133.31, 133.25, 132.12, 131.99, 131.39, 130.73, 128.49, 125.25, 118.70, 118.68, 118.55, 118.53, 116.24, 116.21, 116.09, 116.07, 114.85, 114.56, 93.25, 92.50, 92.24, 91.30, 81.09, 70.76, 17.99, 17.91, 14.40, 17.21, 15.79 15.61, 15.29. MALDI-TOF-MS (% intensity): *m*/*z*: 549.24 (100), 550.2 (55), 551.2 (15). Calcd for $C_{35}H_{31}F_2N_2O_2$ ([M – H]$^-$): 549.24. This compound was further characterized by single-crystal X-ray analysis.

2.1.4. (1,3-Bis(3,4-diethyl-5-phenylethynylpyrrol-2-yl)-1,3-propanedionato-κ^{2}O,O´)[2-(2-pyridinyl-κN)phenyl-κC]platinum, ***2b****.*

According to the literature procedure,[24,25] in a dried round-bottomed flask, [$(PtMe_2)_2(\mu\text{-}SMe_2)_2$] [29] (50 mg, 0.086 mmol) was dissolved in tetrahydrofuran (THF) (1.5 mL) under N_2 atmosphere. To the solution was added 2-phenylpyridine (ppy) (25 μL, 0.16 mmol). The resulting mixture was stirred at room temperature (r.t.) for 1 h, and trifluoromethanesulfonic acid (TfOH) (15 μL, 0.17 mmol) was added dropwise.

The reaction mixture was stirred for 1 h, and then a solution of **1b´** (41.2 mg, 0.080 mmol) and K_2CO_3 (50.6 mg, 0.361 mmol) in THF (5 mL) was added. The mixture was stirred for 3 h. After the removal of the solvent under vacuum, the residue was purified with column chromatography over silica gel (Wakogel C-300; eluent: CH_2Cl_2/*n*-hexane = 3/2) to give **2b** (12.8 mg, 14.8 μmol, 15%) as an orange solid. Silica gel column chromatography and recrystallization processes were conducted under dark condition by covering with aluminum foil. R_f = 0.67 (CH_2Cl_2/*n*-hexane = 3/2 (v/v)). m.p.: 146 °C. ^{1}H NMR (600 MHz, DMSO-d_6, 20 °C): δ (ppm) 11.58 (br, 1H, NH), 11.45 (br, 1H, NH), 9.04 (d, J = 5.4 Hz, 1H, Ar-H), 8.07 (t, J = 7.5 Hz, 1H, Ar-H), 8.02 (d, J = 7.8 Hz, 1H, Ar-H), 7.68 (d, J = 7.8 Hz, 1H, Ar-H), 7.59 (d, J = 7.2 Hz, 1H, Ar-H), 7.55–7.53 (m, 4H, Ar-H), 7.45–7.40 (m, 7H, Ar-H), 7.13 (t, J = 7.2 Hz, 1H, Ar-H), 7.08 (t, J = 6.6 Hz, 1H, Ar-H), 6.31 (s, 1H, bridging CH), 2.94–2.86 (m, 4H, CH_2), 2.60–2.58 (m, 4H, CH_2), 1.26–1.18 (m, 12H, CH_3). UV/vis (CH_2Cl_2, λ_{max}[nm] (ε, 10^4 $M^{-1}cm^{-1}$)): 462 (6.6). MALDI-TOF-MS (% intensity): *m*/*z*: 860.3 (70), 861.4 (100), 862.3 (80). Calcd for $C_{46}H_{40}N_3O_2Pt$ ([M – H]$^-$): 860.28. This compound was further characterized as the Cl^- complex (ion pairs) by single-crystal X-ray analysis.

2.1.5. (1,3-Bis(3,4-diethyl-5-(4-fluorophenyl)ethynylpyrrol-2-yl)-1,3-propanedionato-κ^{2}O,O´)[2-(2-pyridinyl-κN)phenyl-κC]platinum, ***2c****.*

According to the literature procedure,[24,25] in a dried round-bottomed flask, [$(PtMe_2)_2(\mu\text{-}SMe_2)_2$] [29] (39.2 mg, 0.0679 mmol) was dissolved in THF (2 mL) under N_2 atmosphere. To the solution was added ppy (21.1 μL, 0.136 mmol). The resulting mixture was stirred at r.t. for 1 h, and TfOH (15 μL, 0.14 mmol) was added dropwise. The reaction mixture was stirred for 1 h, and then a solution of **1c´** (74.8 mg, 0.136 mmol) and NaOH (5.40 mg, 0.135 mmol) in THF (3.5 mL) and MeOH (0.5 mL) was added. The mixture was stirred for 14 h. After the removal of the solvent under

vacuum, the residue was purified with column chromatography over silica gel (Wakogel C-300; eluent: CH_2Cl_2/*n*-hexane = 3/2) to give **2c** (38.6 mg, 43.0 μmol, 32%) as an orange solid. Silica gel column chromatography and recrystallization processes were conducted under dark condition by covering with aluminum foil. R_f = 0.72 (CH_2Cl_2/*n*-hexane = 3/2 (v/v)). Decomposed at >220 °C without melting. ^{1}H NMR (600 MHz, $CDCl_3$, 20 °C): δ(ppm) 9.14 (br, 1H, NH), 9.01 (d, J = 6.0 Hz, 1H, Ar-H), 8.93 (br, 1H, NH), 7.86 (t, J = 8.4 Hz, 1H, Ar-H), 7.66 (d, J = 7.8 Hz, 1H), 7.62 (d, J = 7.8 Hz, 1H, Ar-H), 7.54–7.49 (m, 5H, Ar-H), 7.30 (t, J = 7.2 Hz, 1H, Ar-H), 7.21 (t, J = 6.9 Hz, 1H, Ar-H), 7.15 (t, J = 6.9 Hz, 1H, Ar-H), 7.08 (t, J = 7.8 Hz, 4H, Ar-H), 6.35 (s, 1H, bridging CH), 2.86–2.80 (m, 4H, CH_2), 2.66–2.62 (m, 4H, CH_2), 1.31–1.23 (m, 12H, CH_3). UV/vis (CH_2Cl_2, λ_{max}[nm] (ε, 10^4 $M^{-1}cm^{-1}$)): 460 (7.9). MALDI-TOF-MS (% intensity): *m*/*z*: 896.2 (64), 897.3 (100), 898.2 (94). Calcd for $C_{46}H_{38}F_2N_3O_2Pt$ ([M – H]$^-$): 897.26. This compound was further characterized as the Cl^- complex (ion pair) by single-crystal X-ray analysis.

2.2. Method for single-crystal X-ray analysis

Crystallographic data are summarized in Table 1. A single crystal of **1c´** was obtained by vapor diffusion of *n*-hexane into a CH_2Cl_2 solution. The data crystal was a yellow block of approximate dimensions 0.135 mm × 0.135 mm × 0.088 mm. A single crystal of **2b**·Cl^--TBA^+ (TBA^+ = tetrabutylammonium) was obtained by vapor diffusion of *n*-hexane into an acetone solution of the mixture of **2b** and TBACl in the 1:1 ratio. The data crystal was a yellow needle of approximate dimensions 0.10 mm × 0.05 mm × 0.01 mm. The data crystal was an orange needle of approximate dimensions 0.182 mm × 0.021 mm × 0.014 mm. A single crystal of **2c**·Cl^--TBA^+ was obtained by vapor

diffusion of *n*-octane into a $CHCl_3$ solution of the mixture of **2c** and TBACl in the 1:1 ratio. A single crystal of **2b**·Cl^--$TPPAu^+$ was obtained by vapor diffusion of *n*-hexane into a THF solution of the mixture of **2b** and tetraphenylporphyrin Au^{III} complex as a Cl^- salt (TPPAuCl) [30] in the 1:1 ratio. The data crystal was a yellow needle of approximate dimensions 0.10 mm × 0.05 mm × 0.02 mm. A single crystal of **2c**·Cl^--$TPPAu^+$ was obtained by vapor diffusion of *n*-hexane into an acetone solution of the mixture of **2c** and TPPAuCl [30] in the 1:1 ratio. The data crystal was an orange needle of approximate dimensions 0.30 mm × 0.30 mm × 0.05 mm. The data of **1c´** and **2b**·Cl^--TPPAu were collected at 90 K on a DECTRIS PILATUS3 CdTe 1M diffractometer with Si (311) monochromated synchrotron radiation (λ = 0.4134 Å) at BL02B1 (SPring-8) [31], and those of **2b**·Cl^--TBA^+, **2c**·Cl^--TBA^+, and **2c**·Cl^--$TPPAu^+$ were collected at 90, 100, and 90 K, respectively, on a DECTRIS EIGER X 1M diffractometer with Si (111) monochromated synchrotron radiation (λ = 0.80977, 0.81070, and 0.81250 Å, respectively) at BL40XU (SPring-8) [32,33]. All the structures were solved by dual-space method. The structures were refined by a full-matrix least-squares method by using a SHELXL 2014 [34] (Yadokari-XG) [35,36]. In each structure, the non-hydrogen atoms were refined anisotropically. CIF files (CCDC-2326910–2326914) can be obtained free of charge from the Cambridge Crystallographic Data Centre via www.ccdc.cam.ac.uk/data_request/cif.

2.3. Computational method

Density functional theory (DFT) calculations of the geometrical optimizations were carried out using the *Gaussian 16* program [37].

2.4. Method for emission spectra, quantum yields, and emission lifetimes

Emission spectra and quantum yields were recorded on a Hitachi F-4500 fluorescence spectrometer and a Hamamatsu Quantum Yields Measurements System for Organic LED Materials C9920-02, respectively. Emission lifetimes were measured using a C7990S system (Hamamatsu Photonics) equipped with a 403-nm excitation laser, producing 62-ps pulses with a repetition rate of 100 kHz.

3. Results and discussions

3.1. Synthesis and characterization

Dipyrrolyldiketone Pt^{II} complex **2a** was synthesized via Pt^{II} complexation of dipyrrolyldiketone **1a´** as a precursor to dipyrrolyldiketone BF_2 complex **1a**. Arylethynyl-substituted dipyrrolyldiketones as key building blocks for the Pt^{II} complexes were prepared by removing a BF_2 unit from the corresponding BF_2 complexes using a modified method [26]. Treatment of α-arylethynyl dipyrrolyldiketone BF_2 complexes **1b**,**c** [27,28] with $LiOH{\cdot}H_2O$ in 1,4-dioxane/water followed by the addition of AcOH afforded dipyrrolyldiketones **1b´**,**c´** with yields of 83% and 87%, respectively. Pt^{II} complexes **2b**,**c** were prepared with yields of 15% and 32%, respectively, by treating **1b´**,**c´** with a mixture of arylpyridine and $[(PtMe_2)_2(SMe_2)_2]$ [29] at r.t. in the presence of TfOH and K_2CO_3 (Figure 2) [38]. The obtained Pt^{II} complexes **2b**,**c** were characterized by ^1H NMR and MALDI-TOF-MS. The complexes **2b**,**c** exhibited red-shifted absorption maxima (λ_{max}) at 462 and 460 nm, respectively, in CH_2Cl_2 compared to unsubstituted **2a** (416 nm) (Figure 3, S5) [24]. Time-dependent (TD)-DFT calculations [37] at PCM-B3LYP/6-31+G(d,p) with LanL2DZ for Pt (CH_2Cl_2) for the optimized structures revealed that the main absorption bands were mainly attributed to the highest occupied molecular orbital (HOMO)-to-

lowest unoccupied molecular orbital (LUMO) transitions, with small contributions from the ligand-to-ligand charge transfer (LLCT) from the dipyrrolyldiketone unit to the arylpyridine ligand and the ligand-to-metal charge transfer (LMCT) (Figure S23,24). Furthermore, in deoxygenated CH_2Cl_2, **2b**,**c** exhibited red-shifted phosphorescence emissions at 600 and 598 nm, respectively, which were red-shifted by ~80 nm compared to that of **2a**, with quantum yields of 0.11 and 0.14, respectively (Figure S32). The emission lifetimes for **2b**,**c** were 17.3 and 8.0 μs, respectively (Figure S34), suggesting similar magnitude for previously reported dipyrrolyldiketone Pt^{II} complexes including **2a** [24,25]. Although dipyrrolyldiketone Pt^{II} complexes in the absence of pyrrole α-substituents, including **2a**, are stable under ambient conditions, π-extended Pt^{II} complexes **2b**,**c** showed degradation over 10 h when kept in solution, converting to the corresponding dipyrrolyldiketones **1b´**,**c´** by Pt^{II} demetallation. Therefore, a detailed evaluation of the solution-state electronic properties over a prolonged time could not be conducted.

3.2. Anion-binding behaviors

Despite slow degradation, the anion-binding behavior of the dipyrrolyldiketone Pt^{II} complexes in solution was preliminarily elucidated by anion-titration experiments via ^{1}H NMR. Upon the addition of 1.3 equivalent of TBACl to **2b** in CD_2Cl_2 (1.0 mM) at –50 °C, the ^{1}H NMR signals of the pyrrole NH and bridging CH at 9.29/9.23 and 6.38 ppm were shifted downfield to 12.62 and 6.61 ppm, respectively, suggesting the formation of [1+1]-type Cl^- complexes as also observed for the dipyrrolyldiketone Pt^{II} complex **2a** (Figure S31) [24,25]. It should be noted that the [2+1]-type anion-binding mode, seen in arylethynyl-substituted BF_2 complexes including **1b** [27,28], was not

observed. This can be attributed to the smaller anion-binding cavity for **2b**·Cl^- than **1b**·Cl^-, as suggested by theoretically optimized structures [37]. The bridging ∠C–C–C angle in the diketone unit of the optimized **2b**·Cl^- was 128.1°, which is larger by 9.1° than that of **1b**·Cl^-, suggesting that the larger Pt^{II} induced the larger ∠ C–C–C angle and resulting smaller anion-binding cavity (Figure S19). The formation of the [1+1]-type Cl^- binding mode was also evaluated using UV/vis absorption spectral changes upon the addition of TBACl in CH_2Cl_2 (2.0×10^{-5} M) (Figure S30). The absorbance at the λ_{max} of 462 and 460 nm for **2a**,**b**, respectively, decreased upon the addition of TBACl, suggesting the inversion of arylethynyl-substituted pyrrole units upon Cl^- binding. A significant decrease in the λ_{max} absorbances was observed in the corresponding BF_2 complexes **1b**,**c** [27,39].

3.3. Solid-state ion-pairing structures

Solid-state ion-pairing assemblies of receptor–anion complexes and countercations were revealed by X-ray analysis of single crystals. The single crystals of **2b**·Cl^--TBA^+ and **2c**·Cl^--TBA^+ were prepared by vapor diffusion of acetone/*n*-hexane and $CHCl_3$/*n*-octane, respectively, for the mixed solutions of the Pt^{II} complexes and TBACl. Single-crystal X-ray analysis of **2b**·Cl^--TBA^+ and **2c**·Cl^--TBA^+ revealed the [1+1]-type Cl^--binding mode using pyrrole N–H···Cl^- and bridging C–H···Cl^- hydrogen-bonding interactions with the N/C(–H)···Cl^- distances of 3.18/3.19 and 3.60 Å (for an independent structure) and 3.28/3.17 and 3.60 Å, respectively (Figure 4, S11,12). The planar Cl^- complexes **2b**·Cl^- and **2c**·Cl^-, showing mean-plane deviations of 0.37/0.49 (two independent structures) and 0.35 Å, respectively, for the planes consisting of arylethynyl-substituted dipyrrolyldiketones and Cl^-, were alternately

arranged with counter TBA^+, forming charge-by-charge columnar structures. The proximally located $Pt^{II}\cdots Pt^{II}$ distance in **2b**·Cl^--TBA^+ and **2c**·Cl^--TBA^+ were 6.73 and 5.78 Å, respectively, indicating the absence of favorable $Pt^{II}\cdots Pt^{II}$ interactions. In both cases, TBA^+ was positioned in close proximity to the dipyrrolyldiketone–Cl^- complex unit. Consequently, the phenylpyridine unit of the Pt^{II} complex was partially stacked with the distances measuring 3.45 and 3.58 Å, respectively. The nearly flat geometries of the square planar Pt^{II} complexes were also indicated by τ_4 values [40] of 0.08/0.09 and 0.09 for **2b**·Cl^- and **2c**·Cl^-, respectively.

Ion-pairing assemblies with π-electronic cations have also been investigated using single-crystal X-ray analysis. Single crystals of **2b**·Cl^--$TPPAu^+$ and **2c**·Cl^--$TPPAu^+$ ($TPPAu^+$: *meso*-tetraphenylporphyrin Au^{III} complex [30]) were prepared by vapor diffusion of THF/*n*-hexane and acetone/*n*-hexane, respectively. $TPPAu^+$ has been used as a planar π-electronic cation for ion-pairing assemblies with anion-responsive π-electronic molecules in their anion complex forms [19,24,41]. In the solid state, **2b**·Cl^- and **2c**·Cl^- formed planar [1+1]-type Cl^--binding structures with hydrogen bonding with the pyrrole-N(–H)$\cdots Cl^-$ and bridging-C(–H)$\cdots Cl^-$ distances of 3.19/3.18 and 3.68 Å and 3.09/3.12 and 3.60 Å, respectively (Figure 5, S13,14). Mean-plane deviations for **2b**·Cl^- and **2c**·Cl^- are 0.20 and 0.28 Å, respectively, which are smaller than those in the ion-pairing assemblies with TBA^+. The smaller mean-plane deviations are attributed to the stacking of the planar anion complexes and $TPPAu^+$. In fact, the distances between the mean planes of the Cl^- complexes and $TPPAu^+$ are 3.91 and 3.61 Å, respectively. Planar units of the phenylpyridine–Pt^{II} units are also stacked with $TPPAu^+$ with the stacking distances of 3.65 and 3.26 Å, respectively, forming charge-by-charge stacking columnar structures. It should be noticed that the planes comprising the phenylpyridine and dipyrrolyldiketone–Cl^- complex units were independently stacked with the

proximally located $TPPAu^+$. The Hirshfeld surface analysis [42] of the stacking structures of phenylpyridine and $TPPAu^+$ showed red and blue triangles arranged in bow-tie shapes on the shape-index surface and a flat region on the curvedness, suggesting characteristic mapping patterns for π–π stacking structures (Figure 6, S17,18).

The charge-by-charge assemblies of planar [1+1]-type anion complexes as pseudo-π-electronic anions and countercations were further analyzed to determine the interaction energies between the components. Energy decomposition analysis (EDA) based on an FMO2-MP2 [43–47] using mixed basis sets including NOSeC-V-TZP for Pt and NOSeC-V-DZP for the other atoms for stacked structure of **2b**·$Cl^–$ and $TPPAu^+$ suggested total interaction energy (E_{tot}) of –203.1 kcal/mol with contributions of electrostatic (E_{es}) and dispersion (E_{disp}) interaction energies of –61.9 and –155.6 kcal/mol (for the larger E_{tot} ion pair), respectively, whereas the E_{tot}, E_{es}, and E_{disp} of the proximally located **2b**·$Cl^–$ and TBA^+ were –170.5, –86.3, and –95.2 kcal/mol, respectively (Figure 7a). The larger absolute value of E_{tot} for **2b**·$Cl^–$-$TPPAu^+$ than **2b**·$Cl^–$-TBA^+ is mainly attributed to the larger E_{disp} value, suggesting the occurrence of effective ${}^i\pi$–${}^i\pi$ interactions between stacked **2b**·$Cl^–$ and $TPPAu^+$ [48]. Similarly, the larger E_{disp} for **2c**·$Cl^–$-$TPPAu^+$ than **2c**·$Cl^–$-TBA^+ resulted in the larger E_{tot} value (Figure 7b). In contrast to dipyrrolyldiketone boron complexes [49], the charge-by-charge assemblies of anion-responsive π-electronic systems with π-electronic cations through ${}^i\pi$–${}^i\pi$ interactions were limited to the Pt^{II} complexes [24,25]. π-Extension of the dipyrrolyldiketone Pt^{II} complexes resulted in the formation of larger π-electronic anions, which can be used as the versatile building units in ion-pairing assemblies.

3. Conclusions

Arylethynyl-substituted dipyrrolyldiketone Pt^{II} complexes, as anion-responsive π-electronic systems, exhibit red-shifted absorption and photoluminescence properties. Single-crystal X-ray analysis revealed charge-by-charge assemblies of anion complexes and countercations. In particular, ion-pairing assemblies with π-electronic cation form effective stacked structures via $^{i}\pi$–$^{i}\pi$ interactions. The stacking of phenylpyridine as a π-electronic ligand for Pt^{II} complexes is also important in ion-pairing assemblies. Further modifications through π-extension and the incorporation of chiral units would lead to the development of phosphorescent ion-pairing materials with chiroptical properties.

Acknowledgements

This work was supported by JSPS KAKENHI Grant Numbers JP18H01968 and JP22H02067 for Scientific Research (B), JP19K05444 for Scientific Research (C), JP23K17951 for Challenging Research (Exploratory), and JP20H05863 for Transformative Research Areas (A) "Condensed Conjugation", and Ritsumeikan Global Innovation Research Organization (R-GIRO) project (2017–22 and 2022–27). Theoretical calculations were partially performed at the Research Center for Computational Science, Okazaki, Japan (Projects: 21-IMS-C077, 22-IMS-C077, and 23-IMS-C069). Synchrotron-radiation analysis was performed at BL40XU (2022A1483 and 2023B1390) and BL02B1 (2021B1808) of SPring-8 with approval from the Japan Synchrotron Radiation Research Institute (JASRI). We thank Dr. Kouhei Ichiyanagi, Dr. Nobuhiro Yasuda, and Dr. Yuiga Nakamura JASRI/SPring-8,

for the single-crystal synchrotron-X-ray analysis and Prof. Hitoshi Tamiaki, Ritsumeikan University, for the various measurements.

Disclosure statement

No potential conflict of interest was reported by the authors.

ORCID

Yohei Haketa http://orcid.org/0000-0003-3824-4986

Hiromitsu Maeda http://orcid.org/0000-0001-9928-1655

References

[1] Ariga K, Fakhrullin R. Materials Nanoarchitectonics from Atom to Living Cell: A Method for Everything. 2022;95:774–795.

[2] Ariga K. Materials Nanoarchitectonics: Collaboration between Chem, Nano and Mat. ChemNanoMat. 2023;9:e202300120.

[3] Samorì P, Cacialli F. editors. Functional Supramolecular Architectures: For Organic Electronics and Nanotechnology. Weinheim: Wiley; 2011.

[4] Koch N. editor. Supramolecular Materials for Opto-Electronics. Cambridge: RSC; 2015.

[5] Yu P, Zhen Y, Dong H, et al. Crystal Engineering of Organic Optoelectronic Materials. Chem. 2019;5:2814–2853.

[6] Kousseff CJ, Halaksa R, Parr ZS, et al. Mixed Ionic and Electronic Conduction in Small-Molecule Semiconductors. Chem Rev. 2022;122:4397–4419.

[7] Chen J, Zhang W, Wang L, et al. Recent Research Progress of Organic Small-Molecule Semiconductors with High Electron Mobilities. Adv Mater. 2023;35:2210772.

[8] Yam VWW, Au VKM, Leung SYL. Light-Emitting Self-Assembled Materials Based on d^8 and d^{10} Transition Metal Complexes. Chem Rev. 2015;115:7589–7728.

[9] Strassner T. Phosphorescent Platinum(II) Complexes with C^C* Cyclometalated NHC Ligands. Acc Chem Res. 2016;49:2680–2689.

[10] Ravotto L, Ceroni P. Aggregation induced phosphorescence of metal complexes: From principles to applications. Coord Chem Rev. 2017;346:62–76.

[11] Puttock EV, Walden MT, Williams JAG. The luminescence properties of multinuclear platinum complexes. Coord Chem Rev. 2018;367:127–162.

[12] Yoshida M, Kato M. Cation-controlled luminescence behavior of anionic cyclometalated platinum(II) complexes. Coord Chem Rev. 2020;408:213194.

[13] Han Y, Gao Z, Wang C, et al. Recent progress on supramolecular assembly of organoplatinum(II) complexes into long-range ordered nanostructures. Coord Chem Rev. 2020;414:213300.

[14] Sun MJ, Liu Y, Zeng W, et al. Photoluminescent Anisotropy Amplification in Polymorphic Organic Nanocrystals by Light-Harvesting Energy Transfer. J Am Chem Soc. 2019;141:6157–6161.

[15] Xu FF, Zeng W, Sun MJ, et al. Organoplatinum(II) Cruciform: A Versatile Building Block to Fabricate 2D Microcrystals with Full-Color and White Phosphorescence and Anisotropic Photon Transport. Angew Chem Int Ed. 2022;61;e202116603.

[16] Ma B, Djurovich PI, Thompson ME. Excimer and electron transfer quenching studies of a cyclometalated platinum complex. Coord Chem Rev. 2005;249:1501–1510.

[17] Komiya N, Okada M, Fukumoto K, et al. Highly Phosphorescent Crystals of Vaulted *trans*-Bis(salicylaldiminato)platinum(II) Complexes. J Am Chem Soc. 2011;133:6493–6496.

[18] Komiya N, Itami N, Naota T. Solid-State Phosphorescence of *trans*-Bis(salicylaldiminato)platinum(II) Complexes Bearing Long Alkyl Chains: Morphology Control towards Intense Emission. Chem Eur J. 2013;19:9497–9505.

[19] Haketa Y, Yamasumi K, Maeda H. π-Electronic ion pairs: building blocks for supramolecular nanoarchitectonics via $^{i}\pi$–$^{i}\pi$ interactions. Chem Soc Rev. 2023;52:7170–7196.

[20] Bwambok DK, El-Zahab B, Challa SK, et al. Near-Infrared Fluorescent NanoGUMBOS for Biomedical Imaging. ACS Nano. 2009;4:3854–3860.

[21] Yang Y, Sun C, Wang S, et al. Counterion-Paired Bright Heptamethine Fluorophores with NIR-II Excitation and Emission Enable Multiplexed Biomedical Imaging. Angew Chem Int Ed. 2022;61:e202117436.

[22] Benson CR, Kacenauskaite L, VanDenburgh KL, et al. Plug-and-Play Optical Materials from Fluorescent Dyes and Macrocycles. Chem. 2020;6:1978–1997.

[23] Kacenauskaite L, Stenspil SG, Olsson AH, et al. Universal Concept for Bright, Organic, Solid-State Emitters–Doping of Small-Molecule Ionic Isolation Lattices with FRET Acceptors. J Am Chem Soc. 2022;144:19981–19989.

[24] Kuno A, Hirata G, Tanaka H, et al. Dipyrrolyldiketone Pt^{II} Complexes: Ion-Pairing π-Electronic Systems with Various Anion-Binding Modes. Chem Eur J. 2021;27:10068–10076.

[25] Haketa Y, Komatsu K, Sei H, et al. Enhanced solid-state phosphorescence of organoplatinum π-systems by ion-pairing assembly. Chem Sci. 2024;15:964–973.

[26] Kuno A, Tohnai N, Yasuda N, et al. Conjunction of Pyrrole and Amide Moieties: Highly Anion-Responsive π-Electronic Molecules Forming Ion-Free and Ion-Pairing Assemblies. Chem Eur J. 2017;23:11357–11365.

[27] Yamakado R, Sakurai T, Matsuda W, et al. π-Electron Systems That Form Planar and Interlocked Anion Complexes and Their Ion-Pairing Assemblies. Chem Eur J. 2016;22:626–638.

[28] Yamakado R, Ashida Y, Sato S, et al. Cooperatively Interlocked [2+1]-Type π-System–Anion Complexes. Chem Eur J. 2017;23:4160–4168.

[29] Hill GS, Irwin MJ, Levy CJ, et al. Platinum(II) Complexes of Dimethyl Sulfide. Inorg Synth. 1998;32:149–151.

[30] Haketa Y, Bando Y, Sasano Y, et al. Liquid Crystals Comprising π-Electronic Ions from Porphyrin–Au^{III} Complexes. iScience. 2019;14:241–256.

[31] Sugimoto K, Ohsumi H, Aoyagi S, et al. Extremely High Resolution Single Crystal Diffractometory for Orbital Resolution using High Energy Synchrotron Radiation at SPring-8. AIP Conf Proc. 2010;1234:887–890.

[32] Yasuda, N, Murayama, H.; Fukuyama, Y, et al. X-ray diffractometry for the structure determination of a submicrometre single powder grain. J Synchrotron Rad. 2009;16:352–357.

[33] Yasuda N, Fukuyama Y, Toriumi K, et al. Submicrometer Single Crystal Diffractometry for Highly Accurate Structure Determination. AIP Conf Proc. 2010;1234:147–150.

[34] Sheldrick G M. Crystal structure refinement with SHELXL. Acta Crystallogr Sect A. 2008;64:112–122.

[35] Wakita K. *Yadokari-XG*, *Software for Crystal Structure Analyses*, 2001.

[36] Kabuto C, Akine S, Nemoto, T, et al. Release of Software (Yadokari-XG 2009) for Crystal Structure Analyses. J Cryst Soc Jpn. 2009;51:218–224.

[37] Frisch MJ, Trucks GW, Schlegel HB, et al. Gaussian 16, Revision C.01. Wallingford CT: Gaussian, Inc.; 2016.

[38] Hudson ZM, Blight BA, Wang S. Efficient and high yield one pot synthesis of cyclometalated platinum (II) β-diketonates at ambient temperature. Org Lett. 2012;14:1700–1703.

[39] The K_a values for **2b**,**c** were estimated to be 700 and 1,300 M^{-1} in CH_2Cl_2, respectively (Figure S30), although they should be roughly estimated due to the slightly decomposed species during titration experiment.

[40] Yang L, Powell DR, Houser RP. Structural variation in copper(I) complexes with pyridylmethylamide ligands: structural analysis with a new four-coordinate geometry index, τ4. Dalton Trans. 2007:955–964.

[41] Tanaka H, Haketa Y, Bando Y, et al. Ion-Pairing Assemblies of Porphyrin–Au^{III} Complexes in Combination with π-Electronic Receptor–Anion Complexes. Chem Asian J. 2020;15:494–498.

[42] Spackman PR, Turner MJ, McKinnon JJ, et al. *CrystalExplorer*: a program for Hirshfeld surface analysis, visualization and quantitative analysis of molecular crystals. J Appl Cryst. 2021;54:1006–1011.

[43] Schmidt MW, Baldridge KK, Boatz JA, et al. General atomic and molecular electronic structure system. J Comput Chem. 1993;14:1347–1363.

[44] Gordon MS, Schmidt MW. In Theory and Applications of Computational Chemistry: The First Forty Years. Dykstra CE, Frenking G, Kim KS, et al. editors. Elsevier, 2005.

[45] Phipps MJS, Fox T, Tautermann CS, et al. Energy decomposition analysis approaches and their evaluation on prototypical protein–drug interaction patterns. Chem Soc Rev. 2015;44:3177–3211.

[46] Report for FMO: Kitaura K, Ikeo E, Asada T, et al. Chem Phys Lett. 1999;313:701–706.

[47] Report for pair interaction energy decomposition analysis (PIEDA): Fedorov DG, Kitaura K. Pair interaction energy decomposition analysis. J Comput Chem. 2007;28:222–237.

[48] Sasano Y, Tanaka H, Haketa Y, et al. Ion-pairing π-electronic systems: ordered arrangement and noncovalent interactions of negatively charged porphyrins. Chem Sci. 2021;12:9645–9657.

[49] Maeda H, Nishimura T, Haketa Y, et al. Ion-Pairing Assemblies of Anion-Responsive π-Electronic Systems Bearing Triazole Moieties Introduced by Click Chemistry. J Org Chem. 2022;87:7818–7825.

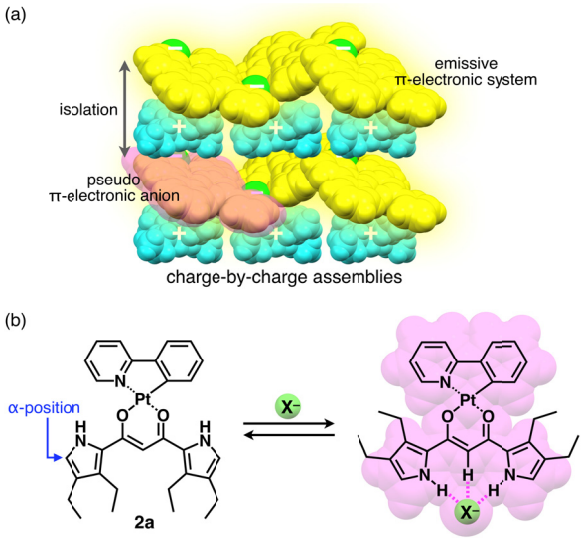

Figure 1. (a) Conceptual diagram for emissive charge-by-charge assembly comprising emissive π-electronic anion and bulky cation and (b) [1+1]-type anion-binding mode of dipyrrolyldiketone Pt^{II} complex **2a**.

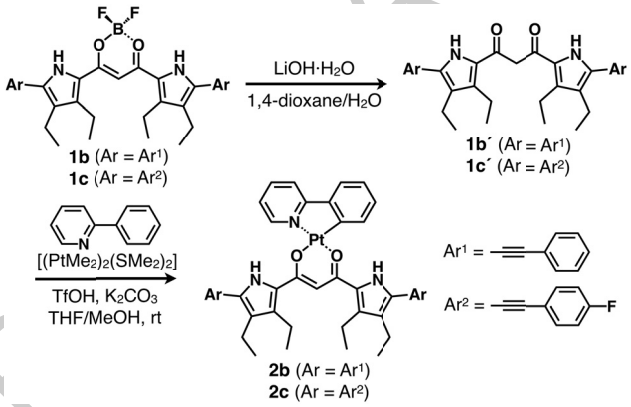

Figure 2. Synthesis of π-extended dipyrrolyldiketone Pt^{II} complexes **2b**,**c**.

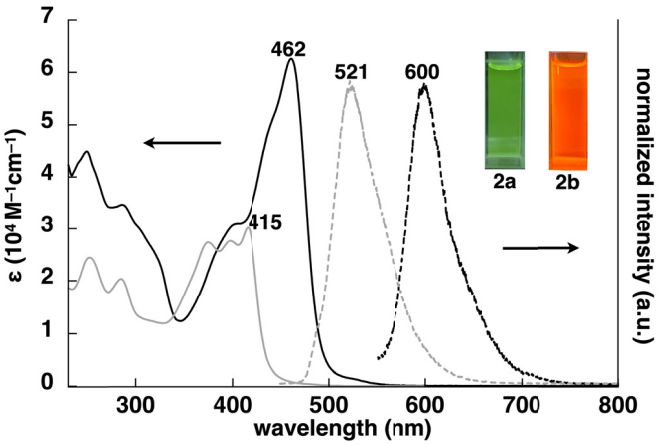

Figure 3. UV/vis absorption spectra (solid lines, CH_2Cl_2) and normalized emission spectra (dashed lines, deoxygenated CH_2Cl_2) with excitations at 415 and 462 nm for **2a** (gray) and **2b** (black), respectively (inset: photographs of **2a**,**b** under UV_{365} (0.02 mM)).

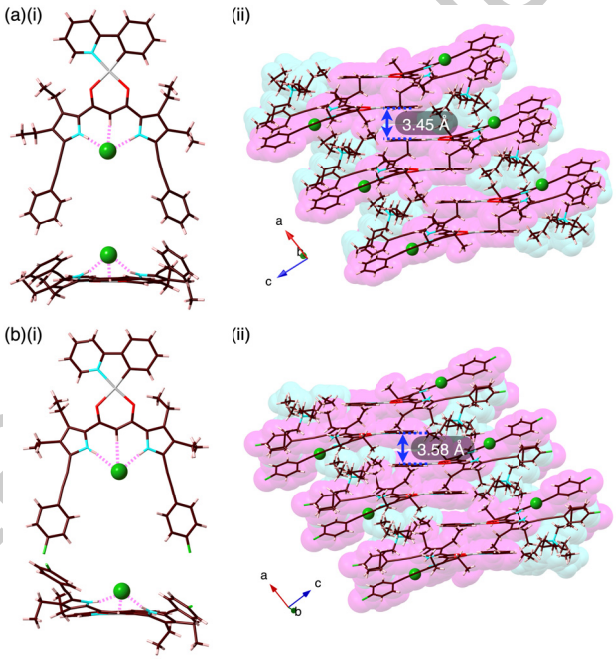

Figure 4. Single-crystal X-ray analysis of (a) **2b**·Cl^--TBA^+ and (b) **2c**·Cl^--TBA^+ ((i) top and side views and (ii) packing diagrams). Atom color code in Figure 4 and the following figures: brown, pink, blue, red, yellow green, green (spherical), and gray refer to carbon, hydrogen, nitrogen, oxygen, fluorine, chlorine, and platinum, respectively.

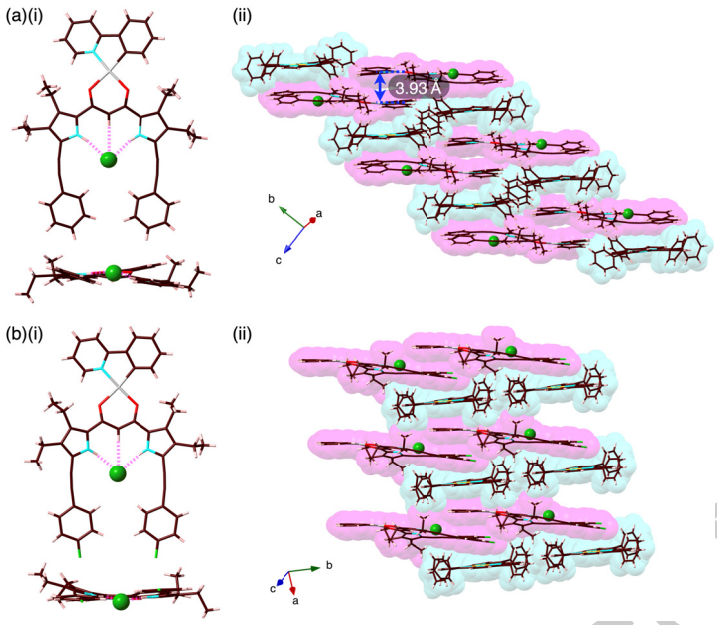

Figure 5. Single-crystal X-ray analysis of (a) **2b**·Cl^{-}-$TPPAu^{+}$ and (b) **2c**·Cl^{-}-$TPPAu^{+}$ ((i) top and side views and (ii) packing diagrams).

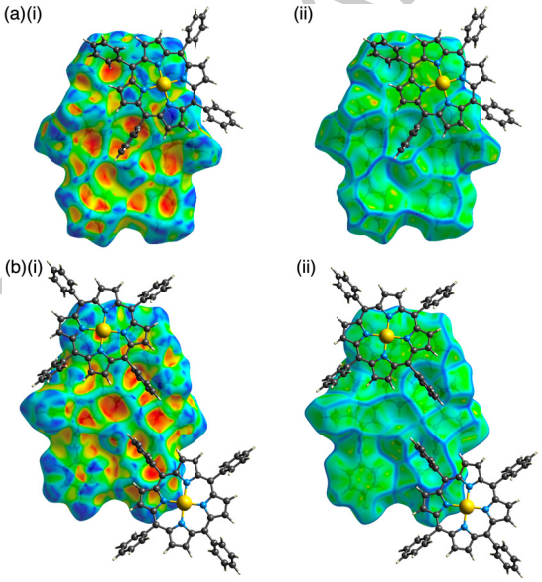

Figure 6. Hirshfeld surface analysis of (a) **2b**·Cl^{-}-$TPPAu^{+}$ and (b) **2c**·Cl^{-}-$TPPAu^{+}$ mapped over (i) shape-index and (ii) curvedness properties for selected stacked structures.

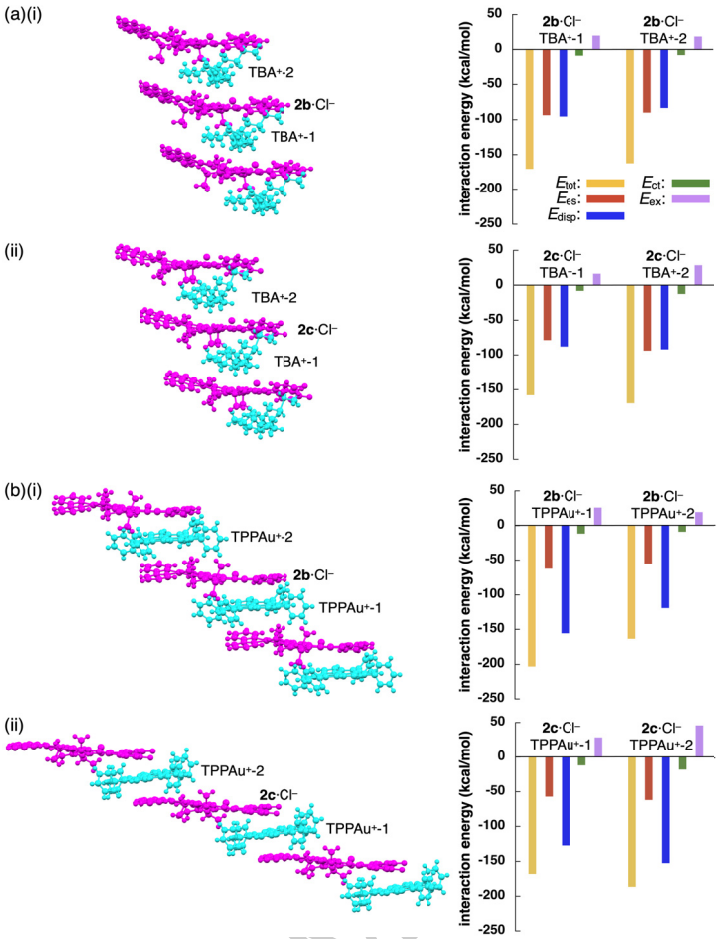

Figure 7. Energy decomposition analysis (EDA) of single-crystal X-ray structures: (a)(i) **2b**·Cl^--TBA^+ and (ii) **2c**·Cl^--TBA^+ and (b)(i) **2c**·Cl^--TBA^+ and (ii) **2c**·Cl^--$TPPAu^+$ (left: packing structures and right: interaction energies for proximally located ion pairs). The anion and cation parts are represented in magenta and cyan colors, respectively.

Table 1 Crystallographic details for **1c´**, **2b**·Cl^--TBA^+, **2c**·Cl^--TBA^+, **2b**·Cl^--$TPPAu^+$, and **2c**·Cl^--$TPPAu^+$.

	1c´	**2b**·Cl^--TBA^+	**2c**·Cl^--TBA^+	**2b**·Cl^--$TPPAu^+$	**2c**·Cl^--$TPPAu^+$
formula	$C_{35}H_{32}F_2N_2O_2$	$C_{46}H_{41}N_3O_2PtCl \cdot C_{16}H_{36}N$	$C_{46}H_{39}N_3O_2F_2PtCl \cdot C_{16}H_{36}N$	$C_{46}H_{41}N_3O_2PtCl \cdot C_{44}H_{28}AuN_4$	$C_{46}H_{39}F_2N_3O_2PtCl \cdot C_{44}H_{28}AuN_4 \cdot 0.5C_3H_6O$
fw	550.62	1140.81	1176.80	1708.02	1773.05
crystal size, mm	0.135 × 0.135 × 0.088	0.10 × 0.05 × 0.01	0.10 × 0.05 × 0.02	0.182 × 0.021 × 0.014	0.30 × 0.30 × 0.05
crystal system	triclinic	triclinic	triclinic	monoclinic	triclinic
space group	*P*-1 (no. 2)	*P*-1 (no. 2)	*P*-1 (no. 2)	$P2_1/c$ (no. 14)	*P*-1 (no. 2)
a, Å	13.939(13)	8.3650(12)	8.6106(4)	21.253(11)	12.9662(9)
b, Å	15.653(15)	15.407(3)	15.5274(8)	13.828(7)	13.3402(9)
c, Å	22.30(2)	43.844(5)	21.8913(9)	26.237(13)	22.4086(18)
α, °	91.48(2)	81.485(8)	103.845(4)	90	105.8934(15)
β, °	90.724(14)	85.275(9)	93.341(4)	108.162(8)	105.4630(15)
γ, °	114.070(11)	86.419(13)	97.512(4)	90	94.294(2)
V, $Å^3$	4440(7)	5562.1(14)	2805.2(2)	7326(6)	3546.9(4)
ρ_{calcd}, gcm^{-3}	1.235	1.362	1.393	1.549	1.660
Z	6	4	2	4	2
T, K	90(2)	90(2)	100(2)	90(2)	90(2)
μ, mm^{-1}	0.036 [a]	3.623 [a]	3.633 [a]	0.989 [a]	5.744 [a]
no. of reflns	91446	52768	33930	199572	38823
no. of unique reflns	19154	20112	12424	16266	12978
variables	1209	1253	535	917	958
λ, Å	0.4134 [a]	0.80977 [a]	0.81250 [a]	0.4134 [a]	0.81070 [a]
R_1 ($I > 2\sigma(I)$)	0.0954	0.1126	0.1351	0.0506	0.0483
wR_2 ($I > 2\sigma(I)$)	0.2691	0.2614	0.3408	0.1088	0.1522
GOF	0.992	1.048	1.045	1.149	1.205

[a] Synchrotron radiation.

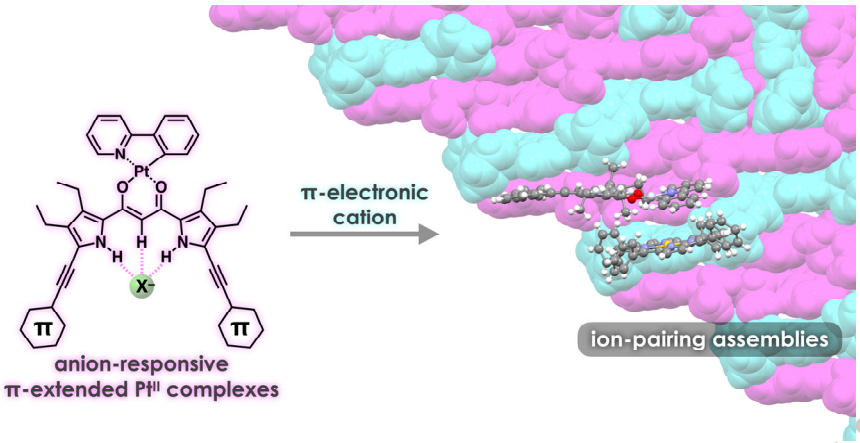

TOC graphic

Statement of Novelty:

Pt^{II} complexes of π-extended dipyrrolyldiketones, introducing arylethynyl substituents, in the form of anion complexes exhibited the formation of charge-by-charge assemblies with π-electronic cations via ${}^{i}\pi-{}^{i}\pi$ interactions.